Published in final edited form as:
ACS Nano. 2012 June 26; 6(6): 5596–5604. doi:10.1021/nn301536n.

Development of Iron Doped Silicon Nanoparticles as Bimodal Imaging Agents

Mani P. Singh[1], **Tonya M. Atkins**[1], **Elayaraja Muthuswamy**[1], **Saeed Kamali**[1], **Chuqiao Tu**[2], **Angelique Y. Louie**[2], and **Susan M. Kauzlarich**[1,*]

[1]Department of Chemistry, University of California, One Shields Avenue, Davis, CA 95616

[2]Department of Biomedical Engineering, University of California, One Shields Avenue, Davis, CA 95616

Abstract

We demonstrate the synthesis of water-soluble allylamine terminated Fe doped Si (Si_{xFe}) nanoparticles as bimodal agents for optical and magnetic imaging. The preparation involves the synthesis of a single source iron containing precursor, Na_4Si_4 with x% Fe (x = 1, 5, 10), and its subsequent reaction with NH_4Br to produce hydrogen terminated Si_{xFe} nanoparticles. The hydrogen-capped nanoparticles are further terminated with allylamine *via* thermal hydrosilylation. Transmission electron microscopy (TEM) indicates that the average particle diameter is ~3.0±1.0 nm. The Si_{5Fe} nanoparticles show strong photoluminescence quantum yield in water (~ 10 %) with significant T_2 contrast (r_2/r_1value of 4.31). Electron paramagnetic resonance (EPR) and Mössbauer spectroscopies indicate that iron in the nanoparticles is in the +3 oxidation state. Analysis of cytotoxicity using the resazurin assay on HepG2 liver cells indicates that the particles have minimal toxicity.

Keywords

Silicon nanoparticles; water soluble; thermal hydrosilylation bimodal imaging agents; iron doping; hepatocytes; cytotoxicity; resazurin assay

The research in the area of nanotechnology has seen immense progress over the years. It is highly exploratory, driven by the demand for better materials for applications in electronics, sensors, catalysis and biomedical science for diagnostics and therapeutics.[1-5] The vast applicability of nanoparticles is a result of their (i) small size which gives them a high surface to volume ratio, (ii) highly tailorable physical properties such as absorbance, emission, magnetism *etc.*, (iii) chemically active surface, and (iv) ability to form highly stable structures.[2] A combination of all the above mentioned properties has led to the application of nanoparticles for diagnostics and therapeutics including metal nanoparticles (Au, Ag),[6, 7] semiconductor nanoparticles (II-VI, III-V, Si)[1, 2, 8] and magnetic nanoparticles (Fe_3O_4, FeCo alloy, MnO, Gd_2O_3).[9-11]

Imaging is an important diagnostic technique and some of the most clinically relevant modalities include optical imaging, MRI (magnetic resonance imaging), and PET (positron electron tomography).[12] While all the imaging techniques have strengths as diagnostics

*To whom correspondence should be addressed.Tel: 530-752-4756; Fax: 530-752-8995. smkauzlarich@ucdavis.edu.

Supporting Information Available: pXRD patterns for the by-product of nanoparticle synthesis, full sweep EPR spectrum and information on the emission of nanoparticles as a function of time, concentration and excitation wavelength is presented in the supporting information. This material is available free of charge *via* the internet at http://pubs.acs.org.

methods, they all suffer from some disadvantages. Optical imaging suffers from low resolution *in vivo* (2-3mm) along with limited skin (tissue penetration, <1cm) while MRI suffers from low sensitivity (mM-μM).[13-15] Multimodality allows for combining the advantages of multiple imaging modalities and may help to overcome the shortcomings of the involved techniques.[13-16] Combining fluorescence and magnetic resonance imaging provides the high sensitivity of optical imaging (nM-pM) and high tissue penetration of MR imaging (no limit).[13, 15] The ability to exploit the multiple modalities in a single imaging agent makes the measurement more accurate and thus, the diagnosis and/or treatment more reliable.[17]

Although it is challenging to blend multiple modalities into a single entity, multimodal nanoparticles offer hope in achieving this goal. The fluorescent properties of semiconductor nanoparticles have proven to be useful for optical imaging while the magnetic properties of iron oxide nanoparticles have been applied for magnetic resonance imaging; it is attractive to consider blending these materials into a single particle.[12, 14] There are examples of multimodal imaging agents available in literature with focus on the development of magneto-fluorescent bimodal imaging agents either by conjugating a fluorescent label to magnetic particles[18, 19] or conjugating a MR-active probe to a fluorescent semiconductor nanoparticle.[12, 20] While these probes have shown success for dual mode imaging, there is concern that the chemically conjugated label can be released, especially under *in vivo* conditions, and mar image interpretation due to the presence of free label. Another approach to designing bimodal imaging agents is to dope an MR-active probe into the nanoparticle.[21, 22] This single entity approach resolves the problems associated with the possible labile nature of chemically bonded groups. Reports have shown successful doping of metal ions into fluorescent semiconductor nanoparticles.[21-23] One factor that weighs into the development of any new material for biological applications is its toxicity, both biological and environmental.[24]

Silicon nanoparticles, which are relatively new in the area of bio-imaging,[25-29] offer a good alternative to the traditional nanoparticles as the silicon based materials have been shown to exhibit minimal toxicity.[25, 30-33] They exhibit a stable fluorescence at different wavelengths based on the synthetic route. They can be synthesized by a variety of methods reported in the literature ranging from reduction of silicon halides,[34] plasma synthesis,[35] high temperature annealing of SiO_x followed by HF etching,[36] electrothermal dispersion of bulk silicon,[25] and *via* microwave assisted reaction of Zintl phases.[37] All the above mentioned synthetic routes produce stable silicon nanoparticles, however many produce nanoparticles that are hydrophobic which makes them unfavorable for bio-imaging unless they can be modified to be water soluble. The reaction of the Zintl phase Na_4Si_4 either in a traditional thermal[38-40] or in a microwave reactor[37] produces hydrogen-capped silicon nanoparticles that can be further reacted to produce water soluble nanoparticles. The benefits of using a Zintl salt to prepare nanoparticles are that it is possible to add paramagnetic ions as a dopant to the starting material and incorporate both photoluminescence and paramagnetism into one small entity. We have reported the synthesis of water soluble manganese doped silicon nanoparticles and shown that both photoluminescence and MRI detection is possible.[26]

In this manuscript, we expand on our previous work and further develop this approach to synthesize highly stable and photoluminescent water soluble propylamine terminated, iron-doped silicon (Si_{xFe}) nanoparticles and demonstrate their application as potential bimodal imaging agents. The nanoparticles were synthesized from $xFe:Na_4Si_4$ which acts as a single source precursor to obtain the desired nanoparticles. The nanoparticles were characterized by a variety of techniques to assess their physical characteristics including core size, fluorescence, EPR, oxidation state of the dopant, relaxivity and magnetic resonance

imaging. The nanoparticles were examined for their toxicity on HepG2 cells and compared to undoped silicon (Si) nanoparticles.

Results and Discussion

The precursors xFe:Na_4Si_4 and the amine terminated iron doped silicon nanoparticles (Si_{xFe}) were synthesized in a similar fashion as we previously described for Mn doped silicon nanoparticles.[26] The reaction between the precursor xFe:Na_4Si_4 and NH_4Br in DMF produced hydrogen terminated nanoparticles which could easily hydrolyze if exposed to air and/or water and hence are not very stable. It is important to coat them with a ligand, which will enhance their stability to air and water. Hydrosilylation has been utilized over the years to stabilize hydrogen terminated silicon surfaces in nanoparticles and thin layers.[34] An unsaturated hydrocarbon (with an additional functional group or otherwise) can replace the surface hydrogen forming a stable Si-C bond thus protecting the surface from hydroxylation. Hydrosilylation has been reported to be catalytically,[29, 41, 42] thermally[43] or photolytically[29, 44] driven. The thermally assisted method is advantageous over the other routes as it avoids extra purification steps (as in the case of catalytic methods) or the longer reaction times[42] (as in the case of UV assisted methods). Allylamine is a short chain ligand which can help maintain a smaller hydrodynamic size for further applications.[45] The absence of a long carbon chain also assists in high water solubility and the terminal amine group lends a wide range of functionality to the nanoparticles for further conjugation to molecules including but not limited to nucleic acids, peptides and therapeutic agents. The amine terminated Si_{xFe} particles prepared by this route are extremely stable to light, air and water over a period of time. Over a period of 15 months, nanoparticles prepared *via* this synthetic route when stored in water on a bench top do not fall out of solution and exhibit a 75% loss in overall quantum yield in comparison to a freshly prepared sample (Figure S1).The synthesis is highly reproducible with the average core size for Si_{xFe} of ~3-4 nm, as determined by TEM (Table 1). A typical TEM image for Si_{5Fe} is shown in Figure 1. Figure 1a shows the average size of the Si_{5Fe} nanoparticles and Figure 1b is the high resolution TEM image of Si_{5Fe} nanoparticle wherein the (2 2 0) lattice plane (1.9 Å) for silicon can be seen as indicated. The inset in Figure 1b depicts the size distribution of the Si_{5Fe} nanoparticles. The HRTEM images confirm the absence of any independent Fe and Si nanoparticles or Fe-Si core-shell structure for these nanoparticles as the difference in the densities of silicon and iron would have been clearly visible in a high resolution TEM image.

The photophysical characteristics of the nanoparticles were measured in aqueous solution. The UV-Vis spectra for the nanoparticles show no significant absorption at wavelengths longer than 600 nm. The photoluminescence (PL) was measured with λ_{ex} = 350 nm for all the samples and yielded an emission peak centered at 430 nm (λ_{em} = 430 nm) as shown in Figure 2. The highest quantum yield of 15% was observed for the sample with the smallest amount of Fe, x = 1, while the sample with x = 5 had a quantum yield of 10%. At x = 10, the quantum yield went down to 1% (Table 1). Loss of quantum yield is not beneficial for the development of a multimodal agent, therefore no magnetic measurements or toxicity assays were performed on the Si_{10Fe} nanoparticles.

Quantitative elemental analysis was performed to determine the extent of iron doping into the nanoparticles. The amount of $Fe(acac)_3$ was increased consistently in the starting mixture with the expectation of achieving higher amounts of iron doping in the nanoparticles. However, analysis of the inductively coupled plasma mass spectrometry (ICP-MS) data indicated that even at the highest amount of $Fe(acac)_3$ in the starting mixture, the iron incorporation into the nanoparticles did not exceed ~1% (Figure 3, Table 1). This observation is indicative of an upper limit to doping levels in the silicon nanoparticle system

and one can hypothesize that the nanoparticle extrudes dopant species in excess of ~1% thus relieving itself of excess strain in the Si nanoparticle structure. As mentioned in the experimental section, the reaction between xFe:Na_4Si_4 and NH_4Br produces a yellow solution which contains the soluble nanoparticles and a black precipitate. As the nanoparticles did not show any increase in the iron content with increasing x the black precipitate (by-product) was analyzed by powder XRD. The powder XRD pattern for the Si_{10Fe} by-product had diffraction peaks corresponding to NaBr, Si, FeSi and Fe whereas that for Si_{1Fe} did not (Figure S2). The Si_{5Fe} sample showed a small peak attributed to FeSi, but no evidence for Fe. These results support the hypothesis that only a limited amount of Fe is soluble in the 3 nm diameter silicon nanoparticles.

Figure 4a shows the X-band EPR spectrum of the amine terminated Si_{1Fe} and Si_{5Fe} nanoparticles measured at 4.2 K. Figure 4a also includes the EPR spectrum for amine terminated undoped silicon nanoparticles for comparison. The singlet at g = 4.3 observed in the case of both Si_{1Fe} and Si_{5Fe} is indicative of isolated high spin Fe(III) centers under rhombic distortion.[46-48] Although there have not been any reports on EPR studies of iron doping into nanoparticles, there are several EPR reports on iron centers trapped in the various glasses, amino acid crystals and zeolite structures.[49-52] Based on these reports it can be concluded that there are isolated iron centers in +3 oxidation state in the core of the nanoparticle. Full sweep EPR spectrum for the undoped silicon nanoparticles and Si_{5Fe} is shown in supporting information (Figure S3). This result is consistent with the iron center as an isolated dopant within the nanoparticle structure and also indicates that there were no clusters of iron in the structure. This result corroborates the absence of core-shell like structures for these nanoparticles as was clearly seen in the HRTEM images (Figure 2).

To further probe the oxidation state of the iron centers in the nanoparticles, ^{57}Fe Mössbauer spectroscopy was carried out on Si_{5Fe} dispersed in ethanol. Mossbauer spectroscopy is a much more sensitive technique and can distinguish between the +2 and +3 states of iron with more accuracy than EPR spectroscopy as the EPR signal for Fe^{2+} is very weak and difficult to detect. The spectrum was least squared fit using Recoil software[53] and the centroid shift is reported with respect to metallic α- iron at room temperature (Figure 4b). The parameters from the fitting are the centroid shift (δ = 0.22±0.01 mm/s), quadrupole splitting (ε = 0.30±0.01 mm/s) and the Lorentzian linewidth (Γ = 0.38±0.01 mm/s).[54] These parameters are in good agreement with Fe^{3+}, indicating 3+ being the only oxidation state for the iron present in the nanoparticles.

The relaxivity measurements were carried out on Si_{1Fe} and Si_{5Fe} at 37 °C (1.4 T) and are shown in Figure 5. The r_2/r_1 for Si_{1Fe} was calculated to be 2.04 while that for Si_{5Fe} it was 4.31. For these nanoparticles to be useful as bimodal imaging agents, along with a measurable quantum yield they should also act as good MRI contrast agents. Magnetic resonance imaging experiments were carried out on Si_{1Fe} (Q.Y. = 15%) and Si_{5Fe} (Q.Y. = 10%). Figure 6a shows the T_2 weighted images for both Si_{1Fe} and Si_{5Fe} nanoparticles dissolved in water. The Si_{5Fe} samples produce a high contrast even at concentrations as low as 1.0 μM whereas Si_{1Fe} did not produce any notable contrast as shown in Figure 6a. Neither of the nanoparticle samples produced noticeable T_1 contrast (data not shown).

The optical emission intensity of the Si_{5Fe} samples was measured at the same iron concentration as for the MRI studied. The samples were excited at λ_{ex} = 350 nm and as the samples entered the non- linear region of absorption at higher concentration, the λ_{max} of emission red shifted with the highest concentration sample (60 μM Fe) to 450 nm (Figure 6b). A plot of the area under the emission intensity curve as a function of concentration and emission λ_{max} as a function of concentration are presented in the supporting information (Figure S4). This shows a quenching of emission intensity and energy shift in the λ_{em} as a

function of concentration of nanoparticle. Organic fluorophores are known to exhibit changes in their photophysical properties as a result of stacking or aggregation.[55, 56] Similar effects have been observed with other fluorescent semiconductor nanoparticles as well to develop switchable fluorescent probes.[57] The change in the λ_{max} for silicon nanoparticles at higher concentration can be applied to confirm the delivery of a payload at a certain site.

Some of the most important criteria that any new material developed for biological applications (including imaging) must fulfill are bio-compatibility, low toxicity and bio-degradability. Various silicon structures have been reported to be highly bio-compatible[31, 33] and are known to degrade to orthosilicic acid $Si(OH)_4$ which can be easily excreted out of the body.[25, 31] However, because nanoparticulates typically are cleared through the liver, retention in the liver is of concern for possible toxicity as the particles degrade.[25, 58] Therefore, it is very important to study the effect of these particles on liver cells. HepG2 cells were treated with the different concentrations (0 – 5mM) of amine terminated Si_{1Fe} and Si_{5Fe} for 4 h, 24 h and 48 h. Similar experiments were repeated with amine terminated undoped silicon nanoparticles to compare the effect of dopant. The cell viability was measured using a resazurin assay. The assay is composed of the resazurin dye, which is non-fluorescent by itself, however, it is reduced to its fluorescent form in the presence of live cells. The cell viability for HepG2 cells treated with Si, Si_{1Fe} and Si_{5Fe} nanoparticles is presented in Figure 7. The nanoparticles show minimal toxicity (cell viability ≥ 85%) to the HepG2 cells throughout the concentration range even at the longest incubation times. Statistical evaluation of the survival rates for the hepatocytes indicates that the survival at 24 h and 48 h is statistically significant ($P<0.05$) in comparison to 4 h incubation times whereas the difference is not significant ($P>0.05$) when comparing the difference in survival rates at 24 h and 48 h incubation times. We have previously shown that the nanoparticles can be detected by imaging after uptake by macrophages.[26] Some previous studies have shown that the amine terminated silicon nanoparticles can have in vitro toxic effects including an increase in the production of intracellular reactive oxygen species measured by a series of complex assays.[33, 59] Resazurin assay is a relatively simpler assay to measure the cytotoxicity and to completely understand the toxicological effects detailed and more complex cell viability assays need to be employed for these nanoparticles. A detailed analysis to assess the cytotoxicity of these nanoparticles is in progress.

Conclusions

Iron doped silicon nanoparticles (Si_{xFe}) have been successfully synthesized from the iron doped sodium silicide precursor ($xFe:Na_4Si_4$). These nanoparticles exhibit extreme stability towards light, air and water. Higher concentrations of the iron dopant in the initial mixture led to extreme loss of photoluminescence, however, at lower concentrations (x = 5%), the nanoparticles were bright and also produced a significant T_2 contrast. These nanoparticles were also of low toxicity as seen in the cell viability assays with cell viability ≥ 85% at concentrations as high as 5 mM. These nanoparticles are promising for bio-imaging applications and the presence of free amines on the surface makes them highly applicable for targeted drug delivery as well. Future work on these nanoparticles is focused on bio-conjugation and an assessment of the toxicity effects of these nanoparticles on other cell lines. These studies will help substantiate the overall minimal toxicity of the particle and also further the applicability of these particles for various other applications in diagnostics and therapeutics.

Experimental

Materials

Reagents for Nanoparticle Synthesis: Sodium hydride powder (NaH, 95%), silicon powder (Si, 99%), anhydrous iron (III) acetylacetonate powder ($Fe(acac)_3$, 99.99 %), allylamine ($C_3H_5NH_2$, 98%), ammonium bromide (NH_4Br, ≥99.99%) and *N,N*-Dimethylformamide (DMF, 99.8%) were purchased either from Sigma Aldrich or Fisher Scientific. $Fe(acac)_3$ and NH_4Br were dried overnight in a vacuum oven. Allylamine (under N_2) and DMF (over sodium metal under vacuum) were distilled prior to use. Na_4Si_4 pellets were obtained from SiGNa Chemistry, Inc. The pellets were crushed to a powder using a mortar and pestle in a N_2 filled glove box. Water was purified using a Nanopure analytical UV water system (18.0 MΩ cm, Barnstead). Reagents for cell culture: Minimum essential medium (MEM) (1X), trypsin 0.05% (1X) with EDTA 4Na, MEM non-essential amino acid solution 10 mM (100X), penicillin-streptomycin (5,000 units of penicillin (base) and 5,000 μg of streptomycin (base)/ml), fetal bovine serum, Dulbecco's phosphate-buffered saline (D-PBS) (1X) and MEM sodium pyruvate solution 100 mM (100X) were purchased from Invitrogen, Inc. Cell Vitality Assay Kit - C_{12} Resazurin/SYTOX® Green was also purchased from Invitrogen, Inc.

Preparation of xFe doped Silicon (Si_{xFe}) Nanoparticles (x=1%, 5%, 10%)

Fe doped silicon nanoparticles were synthesized from the Fe doped sodium silicide ($xFe:Na_4Si_4$) precursor following a previously published procedure.[26, 60] The $xFe:Na_4Si_4$ precursors were prepared according to a modified procedure published for the synthesis of Na_4Si_4.[60] Briefly, a mixture of NaH, Si and $Fe(acac)_3$ in different molar ratios ($m_{NaH} : m_{Si} : m_{Fe} = 1.9: (1-x) : x$, and x = 1 %, 5 %, 10 %) were milled for 30 min in a high-energy Spex 8000 M mill using a tungsten carbide milling vial (volume = 55 mL) and three tungsten carbide balls (one 11.2 mm and two 7.9 mm diameter). The milled mixture was placed in a N_2 filled glove box and transferred to an alumina crucible. The crucible was covered with an alumina cover and placed in a quartz tube with stopcock adapters. The quartz tube was placed in a tube furnace and attached by means of the stopcock adapters to an argon flow at one end and a bubbler at the other. The apparatus was heated at 420 °C for 48 h followed by an additional 12 h at 500 °C under a constant flow of argon. The product was cooled to room temperature under flowing argon and transferred to the glove box for further use and storage.

To synthesize the nanoparticles, 0.2 g $xFe:Na_4Si_4$ and 0.4 g NH_4Br were added to a 250 mL Schlenk flask with a Teflon coated stir bar in the N_2 filled glove box. The flask was brought out of the glove box and placed under N_2 on a Schlenk line. 100mL of degassed DMF was cannulated into the flask and the mixture was refluxed for 8-12 h in order to produce hydrogen terminated Fe doped silicon particles. The reaction was considered complete when there was no more ammonia gas indicated with a pH strip at the exit bubbler. The reaction mixture is then cooled to room temperature and 2 mL of degassed allylamine is added to the flask and the reaction mixture was refluxed again for 4-6 h in order to produce propylamine terminated nanoparticles *via* thermal hydrosilylation. The product, which was a yellow solution with a black precipitate, was cooled to room temperature and transferred to centrifuge tubes. The contents were centrifuged at 8000 rpm for 20 min. The yellow supernatant was transferred into a round bottom flask while the black precipitate was dried in a vacuum oven overnight for further characterization. The supernatant was evaporated using a Buchi rotary evaporator when 10 mL of nanopure water (npH_2O) was added to the flask and the solution evaporated again. This step was repeated to completely remove DMF (4-5 times) followed by addition of 10 mL of npH_2O.The solution was dialyzed against npH_2O for 2-4 h to remove any excess reagents and water soluble impurities. The contents

of the dialysis bag were then filtered using a 0.45 μm filter. The filtrate was brought to dryness using the rotary evaporator. The product was dissolved in 10 mL of npH_2O (or in DMF for EPR) and used for further characterization and experiments. Amine terminated silicon nanoparticles (undoped) were synthesized and purified in a similar manner using Na_4Si_4 as the starting material.

CAUTION

NaH, Na_4Si_4, and xFe:Na_4Si_4 are highly reactive to air and moisture hence must be handled under an inert atmosphere with care.

Characterization

The black precipitate from the Si_{xFe} nanoparticle syntheses was analyzed by powder X-ray diffraction (XRD) on a Bruker D8 Advance X-ray diffractometer with Cu*K*α radiation (λ = 1.54178 Å).The core size for the nanoparticles was determined by transmission electron microscopy on a JEOL 2500SE Schottky emitter microscope operating at 200 kV and equipped with a Gatan multiscan camera. TEM samples were prepared by dropping a methanol solution of the nanoparticle on a holey-carbon-coated, 400-mesh electron microscope grids and drying them under a light bulb overnight. High resolution TEM (HRTEM) images were collected on the same instrument and the grids were prepared in a manner similar to that for the low resolution image. Elemental analysis to determine the amount of iron doping in the nanoparticles was performed on ICP quadrupole mass spectrometers (ICP-MS, Agilent Technologies 7500ce). Quantum yield measurements on an aqueous solution of nanoparticles were performed by measuring the photoluminescence (PL) spectra on a FluoroMax-3P fluorometer and UV-Vis spectra on a Shimadzu UV-1700 PharmaSpec spectrometer. The quantum yields for Si_{xFe} particles are reported with respect to quinine sulfate standard dissolved in 0.1 M H_2SO_4 and excited at 350 nm.

Longitudinal (T_1) and transverse (T_2) relaxation times were measured at 60 MHz (1.4 T), pH 7.2 and 37 °C on a Bruker Minispec mq60 (Bruker, Billerica, MA).The solutions of Si_{xFe} nanoparticles were prepared by dissolving the appropriate amount of samples in npH_2O. Each solution was incubated at 37 °C for 10 min before measurement. The longitudinal (r_1) and transverse (r_2)relaxivity were obtained by calculating the slope of the line for plots of $1/T_1$ *vs.* [Fe] and $1/T_2$ vs. [Fe] respectively. MRI was performed on BrukerAvance I Console (400 MHz (9.4 T), 21 °C, Bruker, Billerica, MA). For the T_1 measurements, TR = 1500 ms, TE = 8 ms, while for the T_2 measurements TR = 1000 ms and TE = 210 ms. The magnet was equipped with the standard gradient set (95 mTm^{-1} maximum gradient) and 30 mm internal diameter SAW volume coil made by M2M Imaging Corp, Ohio. For all images a flash- 2D sequence was used with a field view (FOV) of 3.2 × 3.2 cm^2, slice thickness 1.0 mm, and a 128 × 128 matrix.

The electron paramagnetic resonance (EPR) spectra for the samples were collected on a Bruker ECS106 X-Band spectrometer, equipped with an Oxford Instruments liquid helium cryostat. Typical experimental conditions were frequency 9.68 GHz, temperature 4.2 K, modulation amplitude 10 G, microwave power 0.50 m, conversion time 40.96 ms, time constant 40.96 ms, average of 10 scans. Samples were dissolved in DMF.[57] Fe Mössbauer spectroscopy was performed at 80 K using a SEE Co. MS4 spectrometer equipped with a Janis SVT-400 cryostat. The radioactive source was ^{57}Co in Rh matrix maintained at room temperature. The Si_{5Fe} sample dissolved in DMF was poured into the sample cup and frozen under liquid N_2 to get a 2 mm thick sample for the measurement. The spectrum was least squared fit using Recoil software[53] and the values for metallic α-iron were used to report the centroid shift for the sample.

Toxicity assay

Hepatic cells (HepG2 cells, from ATCC) were maintained in MEM supplemented with 10% FBS, 200 U/mL penicillin, 200 μg/mL streptomycin, 1 mM sodium pyruvate, and 1 mM non-essential amino acids at 37 °C in a humidified 5% CO_2 atmosphere. The cells were released from the culture flask using 0.05% trypsin and resuspended in 13 mL of supplemented MEM. 10 μL of the suspension was loaded on a hemacytometer to determine the cell density. Appropriate dilution was carried out to obtain a cell density of 5×10^4 cell/mL of the suspension. Cell were plated into a 96 well plate at 200 μL of the cell suspension per well. Appropriate amount of dried nanoparticles (Si_{xFe} or Si nanoparticles) were dissolved in supplemented MEM to get a stock solution with 5 mM silicon concentration as determined by ICP-MS. This molar concentration can be converted to g/L (mass/volume) by considering a 3 nm particle comprised of a total of 963 silicon atoms and a 100% surface coverage (275 surface silicon atoms) by the propylamine ligand.[61] The cells in the well plate were incubated with the nanoparticle solution 0, 0.02, 0.2, 0.5 and 5 mM concentrations for 4 h. The lower concentration [Si] solutions were prepared by serial dilution of the 5 mM stock solution. The cell viability was determined using a resazurin assay. For this, 5 mM resazurin solution was prepared in DMSO which was further diluted to 5 μM using the supplemented MEM. For the 4 h time point the media was removed from each well and the cells were washed with 1× PBS (3×200 μL) followed by the addition of 200 μL of 5 μM resazurin solution to each well. The well plate was then placed on Safire^2 monochromator microplate reader (Tecan Austria G.M.B.H., Austria), λ_{ex} = 563 nm and λ_{em} = 587 nm to measure the fluorescence. The cell viability was assessed based on the relative fluorescent signal in comparison to the control well. The same experiment was repeated for the 24 h and 48 h time point for the cell viability.

Supplementary Material

Refer to Web version on PubMed Central for supplementary material.

Acknowledgments

We recognize the support from NIH for funding this work through EB008576-01. We would like to thank Dr. J.H. Walton (UC Davis NMR Facility and CalEPR) for the MRI and EPR experiments and Prof. A. Revzin (Department of Biomedical Engineering, UC Davis) for supplying the HepG2 cells.

References

1. Gao XH, Cui YY, Levenson RM, Chung LWK, Nie SM. *In Vivo* Cancer Targeting and Imaging with Semiconductor Quantum Dots. Nat. Biotechnol. 2004; 22:969–976. [PubMed: 15258594]
2. Alivisatos P. The Use of Nanocrystals in Biological Detection. Nat. Biotechnol. 2004; 22:47–52. [PubMed: 14704706]
3. Tao AR, Habas S, Yang PD. Shape Control of Colloidal Metal Nanocrystals. Small. 2008; 4:310–325.
4. Astruc D, Lu F, Aranzaes JR. Nanoparticles as Recyclable Catalysts: The Frontier Between Homogeneous and Heterogeneous Catalysis. Angew. Chem., Int. Ed. 2005; 44:7852–7872.
5. Shipway AN, Katz E, Willner I. Nanoparticle Arrays on Surfaces for Electronic, Optical, and Sensor Aapplications. Chem. Phys. Chem. 2000; 1:18–52.
6. Huang XH, Jain PK, El-Sayed IH, El-Sayed MA. Gold Nanoparticles: Interesting Optical Properties and Recent Applications in Cancer Diagnostic and Therapy. Nanomedicine. 2007; 2:681–693. [PubMed: 17976030]
7. Jiang W, Kim BYS, Rutka JT, Chan WCW. Nanoparticle-Mediated Cellular Response is Size-Dependent. Nat. Nanotechnol. 2008; 3:145–150. [PubMed: 18654486]

8. Michalet X, Pinaud FF, Bentolila LA, Tsay JM, Doose S, Li JJ, Sundaresan G, Wu AM, Gambhir SS, Weiss S. Quantum Dots for Live Cells, *In Vivo* Imaging, and Diagnostics. Science. 2005; 307:538–544. [PubMed: 15681376]
9. Roberts D, Zhu WL, Frommen CM, Rosenzweig Z. Synthesis of Gadolinium Oxide Magnetoliposomes for Magnetic Resonance Imaging. J. Appl. Phys. 2000; 87:6208–6210.
10. Na HB, Lee JH, An KJ, Park YI, Park M, Lee IS, Nam DH, Kim ST, Kim SH, Kim SW, et al. Development of A T_1 Contrast Agent for Magnetic Resonance Imaging Using MnO Nanoparticles. Angew. Chem., Int. Ed. 2007; 46:5397–5401.
11. Hao R, Xing R, Xu Z, Hou Y, Gao S, Sun S. Synthesis, Functionalization, and Biomedical Applications of Multifunctional Magnetic Nanoparticles. Adv. Mater. 2010; 22:2729–2742. [PubMed: 20473985]
12. Louie A. Multimodality Imaging Probes: Design and Challenges. Chem. Rev. 2010; 110:3146–3195. [PubMed: 20225900]
13. Weissleder R, Pittet MJ. Imaging in The Era of Molecular Oncology. Nature. 2008; 452:580–589. [PubMed: 18385732]
14. Jennings LE, Long NJ. 'Two is Better Than One'-Probes for Dual-Modality Molecular Imaging. Chem. Commun. 2009; 24:3511–3524.
15. Cheon J, Lee JH. Synergistically Integrated Nanoparticles as Multimodal Probes for Nanobiotechnology. Accounts Chem. Res. 2008; 41:1630–1640.
16. Kobayashi H, Longmire MR, Ogawa M, Choyke PL. Rational Chemical Design of The Next Generation of Molecular Imaging Probes Based on Physics and Biology: Mixing Modalities, Colors and Signals. Chem. Soc. Rev. 2011; 40:4626–4648. [PubMed: 21607237]
17. Kircher MF, Mahmood U, King RS, Weissleder R, Josephson L. A Multimodal Nanoparticle for Preoperative Magnetic Resonance Imaging and Intraoperative Optical Brain Tumor Delineation. Cancer Research. 2003; 63:8122–8125. [PubMed: 14678964]
18. Josephson L, Kircher MF, Mahmood U, Tang Y, Weissleder R. Near-Infrared Fluorescent Nanoparticles as Combined MR/Optical Imaging Probes. Bioconjugate Chem. 2002; 13:554–560.
19. Veiseh O, Sun C, Gunn J, Kohler N, Gabikian P, Lee D, Bhattarai N, Ellenbogen R, Sze R, Hallahan A, et al. Optical and MRI Multifunctional Nanoprobe for Targeting Gliomas. Nano Lett. 2005; 5:1003–1008. [PubMed: 15943433]
20. Mulder WJM, Koole R, Brandwijk RJ, Storm G, Chin PTK, Strijkers GJ, Donega CD, Nicolay K, Griffioen AW. Quantum Dots with A Paramagnetic Coating As A Bimodal Molecular Imaging Probe. Nano Lett. 2006; 6:1–6. [PubMed: 16402777]
21. Wang S, Jarrett BR, Kauzlarich SM, Louie AY. Core/Shell Quantum Dots with High Relaxivity and Photoluminescence for Multimodality Imaging. J. Am. Chem. Soc. 2007; 129:3848–3856. [PubMed: 17358058]
22. Beaulac R, Schneider L, Archer PI, Bacher G, Gamelin DR. Light-Induced Spontaneous Magnetization in Doped Colloidal Quantum Dots. Science. 2009; 325:973–976. [PubMed: 19696345]
23. Magana D, Perera SC, Harter AG, Dalal NS, Strouse GF. Switching-On Superparamagnetism in Mn/CdSe Quantum Dots. J. Am. Chem. Soc. 2006; 128:2931–2939. [PubMed: 16506772]
24. Lewinski N, Colvin V, Drezek R. Cytotoxicity of Nanoparticles. Small. 2008; 4:26–49. [PubMed: 18165959]
25. Park JH, Gu L, von Maltzahn G, Ruoslahti E, Bhatia SN, Sailor MJ. Biodegradable Luminescent Porous Silicon Nanoparticles for *In Vivo* Applications. Nat. Mater. 2009; 8:331–336. [PubMed: 19234444]
26. Tu CQ, Ma XC, Pantazis P, Kauzlarich SM, Louie AY. Paramagnetic, Silicon Quantum Dots for Magnetic Resonance and Two-Photon Imaging of Macrophages. J. Am. Chem. Soc. 2010; 132:2016–2023. [PubMed: 20092250]
27. Erogbogbo F, Yong KT, Roy I, Hu R, Law WC, Zhao WW, Ding H, Wu F, Kumar R, Swihart MT, et al. *In Vivo* Targeted Cancer Imaging, Sentinel Lymph Node Mapping and Multi-Channel Imaging with Biocompatible Silicon Nanocrystals. ACS Nano. 2011; 5:413–423. [PubMed: 21138323]

28. Erogbogbo F, Yong KT, Roy I, Xu GX, Prasad PN, Swihart MT. Biocompatible Luminescent Silicon Quantum Dots for Imaging of Cancer Cells. ACS Nano. 2008; 2:873–878. [PubMed: 19206483]
29. Shiohara A, Prabakar S, Faramus A, Hsu CY, Lai PS, Northcote PT, Tilley RD. Sized Controlled Synthesis, Purification, and Cell Studies with Silicon Quantum Dots. Nanoscale. 2011; 3:3364–3370. [PubMed: 21727983]
30. Alvarez SD, Derfus AM, Schwartz MP, Bhatia SN, Sailor MJ. The Compatibility of Hepatocytes with Chemically Modified Porous Silicon with Reference to *In Vitro* Biosensors. Biomaterials. 2009; 30:26–34. [PubMed: 18845334]
31. Chin V, Collins BE, Sailor MJ, Bhatia SN. Compatibility of Primary Hepatocytes with Oxidized Nanoporous Silicon. Adv. Mater. 2001; 13:1877–1880.
32. Nagesha DK, Whitehead MA, Coffer JL. Biorelevant Calcification and Non-Cytotoxic Behavior in Silicon Nanowires. Adv. Mater. 2005; 17:921–926.
33. Ruizendaal L, Bhattacharjee S, Pournazari K, Rosso-Vasic M, de Haan LHJ, Alink GM, Marcelis ATM, Zuilhof H. Synthesis and Cytotoxicity of Silicon Nanoparticles with Covalently Attached Organic Monolayers. Nanotoxicology. 2009; 3:339–347.
34. Warner JH, Hoshino A, Yamamoto K, Tilley RD. Water-Soluble Photoluminescent Silicon Quantum Dots. Angew. Chem. Int. Ed. 2005; 44:4550–4554.
35. Mangolini L, Thimsen E, Kortshagen U. High-Yield Plasma Synthesis of Luminescent Silicon Nanocrystals. Nano Lett. 2005; 5:655–659. [PubMed: 15826104]
36. Hessel CM, Henderson EJ, Veinot JGC. Hydrogen Silsesquioxane: A Molecular Precursor for Nanocrystalline Si-SiO_2 Composites and Freestanding Hydride-Surface-Terminated Silicon Nanoparticles. Chem. Mater. 2006; 18:6139–6146.
37. Atkins TM, Thibert A, Larsen DS, Dey S, Browning ND, Kauzlarich SM. Femtosecond Ligand/Core Dynamics of Microwave-Assisted Synthesized Silicon Quantum Dots in Aqueous Solution. J. Am. Chem. Soc. 2011; 133:20664–20667. [PubMed: 22103236]
38. Zhang XM, Neiner D, Wang SZ, Louie AY, Kauzlarich SM. A New Solution Route to Hydrogen-Terminated Silicon Nanoparticles: Synthesis, Functionalization and Water Stability. Nanotechnology. 2007; 18:095601(1)–095601(6).
39. Manhat BA, Brown AL, Black LA, Ross JBA, Fichter K, Vu T, Richman E, Goforth AM. One-Step Melt Synthesis of Water-Soluble, Photoluminescent, Surface-Oxidized Silicon Nanoparticles for Cellular Imaging Applications. Chem. Mater. 2011; 23:2407–2418.
40. Neiner D, Chiu HW, Kauzlarich SM. Low-Temperature Solution Route to Macroscopic Amounts of Hydrogen Terminated Silicon Nanoparticles. J. Am. Chem. Soc. 2006; 128:11016–11017. [PubMed: 16925406]
41. Rosso-Vasic M, Spruijt E, van Lagen B, De Cola L, Zuilhof H. Alkyl-Functionalized Oxide-Free Silicon Nanoparticles: Synthesis and Optical Properties. Small. 2008; 4:1835–1841. [PubMed: 18752208]
42. Clark RJ, Dang MKM, Veinot JGC. Exploration of Organic Acid Chain Length on Water-Soluble Silicon Quantum Dot Surfaces. Langmuir. 2010; 26:15657–15664. [PubMed: 20815392]
43. Anthony R, Kortshagen U. Photoluminescence Quantum Yields of Amorphous and Crystalline Silicon Nanoparticles. Phys. Rev. B. 2009; 80:115407(1)–115407(6).
44. Kelly JA, Veinot JGC. An Investigation into Near-UV Hydrosilylation of Freestanding Silicon Nanocrystals. ACS Nano. 2010; 4:4645–4656. [PubMed: 20731446]
45. Veiseh O, Gunn JW, Zhang M. Design and Fabrication of Magnetic Nanoparticles for Targeted Drug Delivery and Imaging. Adv. Drug Deliver. Rev. 2010; 62:284–304.
46. Castner T, Newell GS, Holton WC, Slichter CP. Note on the Paramagnetic Resonance of Iron in Glass. J. Chem. Phys. 1960; 32:668–673.
47. Harrop TC, Tyler LA, Olmstead MM, Mascharakla PK. Change in the Spin State of an Fe-III Center upon One N-to-O Switch in the Coordination of a 2,6-Pyridinedicarboxamido Unit: The Effect of Methyl Thioether and Methyl Ether Appendages at the Ligand Periphery. Eur. J. Inorg. Chem. 2003; 3:475–481.
48. Wickman HH, Klein MP, Shirley DA. Paramagnetic Resonance of Fe^{3+} in Polycrystalline Ferrichrome A. J. Chem. Phys. 1965; 42:2113–2117.

49. Nozaki C, Lugmair CG, Bell AT, Tilley TD. Synthesis, Characterization, and Catalytic Performance of Single-Site Iron(III) Centers on The Surface of SBA-15 Silica. J. Am. Chem. Soc. 2002; 124:13194–13203. [PubMed: 12405848]
50. Zhilinskaya EA, Delahay G, Mauvezin M, Coq B, Aboukais A. EPR Investigation of Fe-Exchanged Beta-Zeolites. Langmuir. 2003; 19:3596–3602.
51. Ferretti AM, Barra AL, Forni L, Oliva C, Schweiger A, Ponti A. Electron Paramagnetic Resonance Spectroscopy of Iron(III)-Doped MF1 Zeolite. 1. Multifrequency CW-EPR. J. Phys. Chem. B. 2004; 108:1999–2005.
52. SivaRamaiah G, Lin JR, Pan YM. Electron Paramagnetic Resonance Spectroscopy of Fe^{3+} Ions in Amethyst: Thermodynamic Potentials and Magnetic Susceptibility. Phys. Chem. Miner. 2011; 38:159–167.
53. Lagarec, K.; Rancourt, DC. Recoil, Mössbauer Spectral Analysis Software for Windows, 1.0. 1998.
54. Murad, E.; Cashion, J. Mössbauer Spectroscopy of Environmental Materials and Their Industrial Utilization. Kluwer Academic Publishers; 2004.
55. West W, Pearce S. Dimeric State of Cyanine Dyes. J. Phys. Chem. 1965; 69:1894–1903.
56. Armitage, BA. Cyanine Dye-DNA Interactions: Intercalation, Groove Binding, and Aggregation. In: Waring, MJ.; Chaires, JB., editors. Top. Curr. Chem. Vol. Vol. 253. Springer-Verlag Berlin; Berlin: 2005. p. 55-76.
57. Liu J, Yang X, Wang K, Yang R, Ji H, Yang L, Wu C. A Switchable Fluorescent Quantum Dot Probe Based on Aggregation/Disaggregation Mechanism. Chem. Commun. 2011; 47:935–937.
58. Tu C, Ma X, House A, Kauzlarich SM, Louie AY. PET Imaging and Biodistribution of Silicon Quantum Dots in Mice. ACS Med. Chem. Lett. 2011; 2:285–288. [PubMed: 21546997]
59. Bhattacharjee S, de Haan LHJ, Evers NM, Jiang X, Marcelis ATM, Zuilhof H, Rietjens I, Alink GM. Role of Surface Charge and Oxidative Stress in Cytotoxicity of Organic Monolayer-Coated Silicon Nanoparticles Towards Macrophage NR8383 cells. Part. Fibre Toxicol. 2010; 7:25(1)–25(12). [PubMed: 20831820]
60. Ma XC, Xu F, Atkins TM, Goforth AM, Neiner D, Navrotsky A, Kauzlarich SM. A Versatile Low Temperature Synthetic Route to Zintl Phase Precursors: Na_4Si_4, Na_4Ge_4 and K_4Ge_4 as Examples. Dalton T. 2009; 46:10250–10255.
61. Zou J, Sanelle P, Pettigrew KA, Kauzlarich SM. Size and Spectroscopy of Silicon Nanoparticles Prepared Via Reduction of $SiCl_4$. Journal of Cluster Science. 2006; 17:565–578.

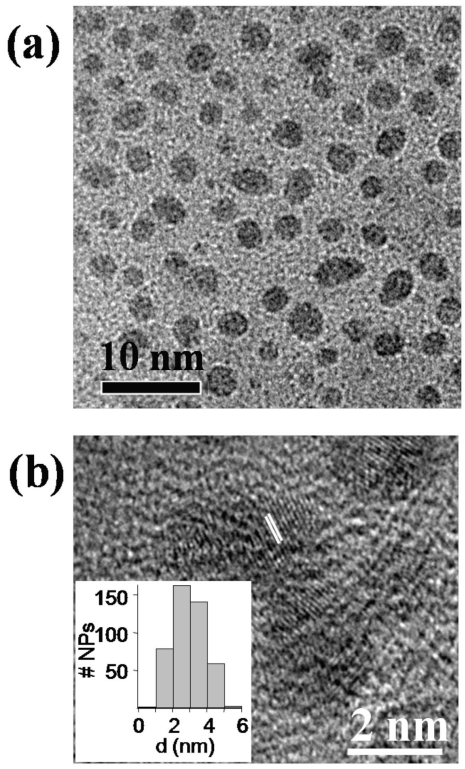

Figure 1.
(a) TEM image of Si_{5Fe}, and **(b)** (2 2 0) Si plane in the nanoparticles with the measured distance between the planes in the nanoparticles being 1.9 Å. Inset in **(b)** depicts the size distribution of the Si_{5Fe} nanoparticles as measured by TEM.

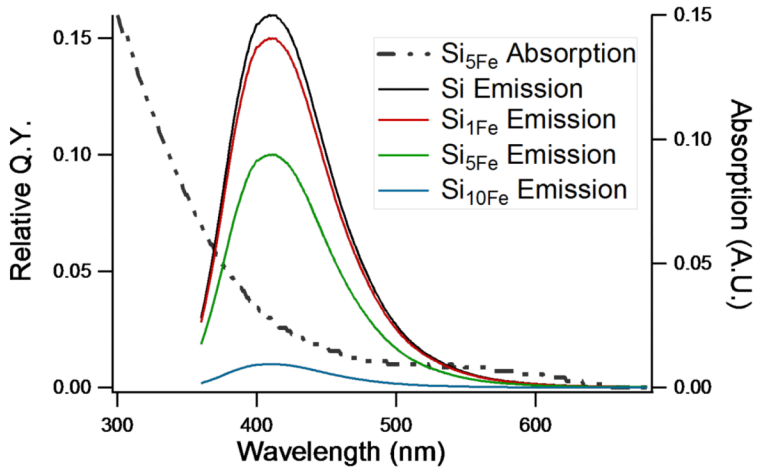

Figure 2.

Relative quantum yield (Q.Y.) for amine terminated water soluble Si and Si_{xFe} nanoparticles. The absorption spectrum for Si_{5Fe} is shown as well. Si, Si_{1Fe} and Si_{10Fe} nanoparticles exhibit a similar absorption profile.

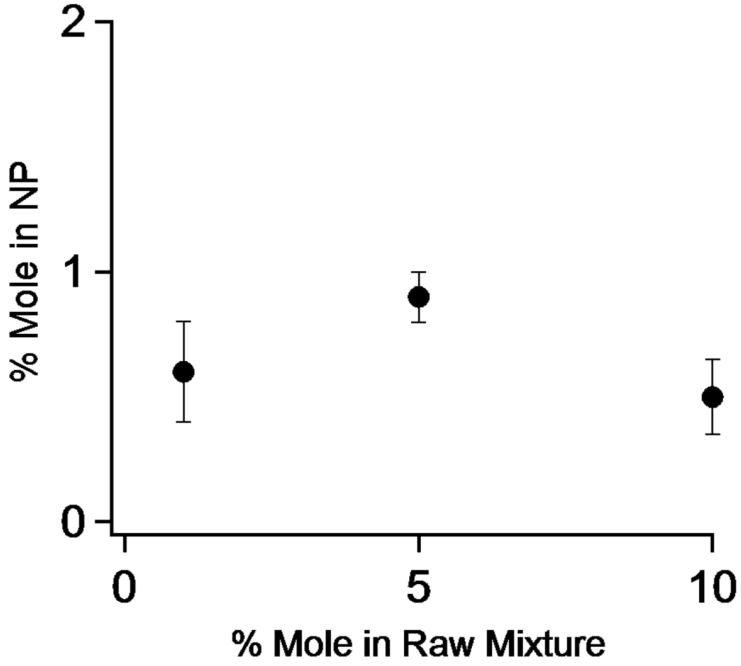

Figure 3.
Plot of the amount of dopant (Fe^{3+}) in the Si_{xFe} nanoparticles *vs.* the amount of Fe^{3+} in the initial milled mixture (n=3).

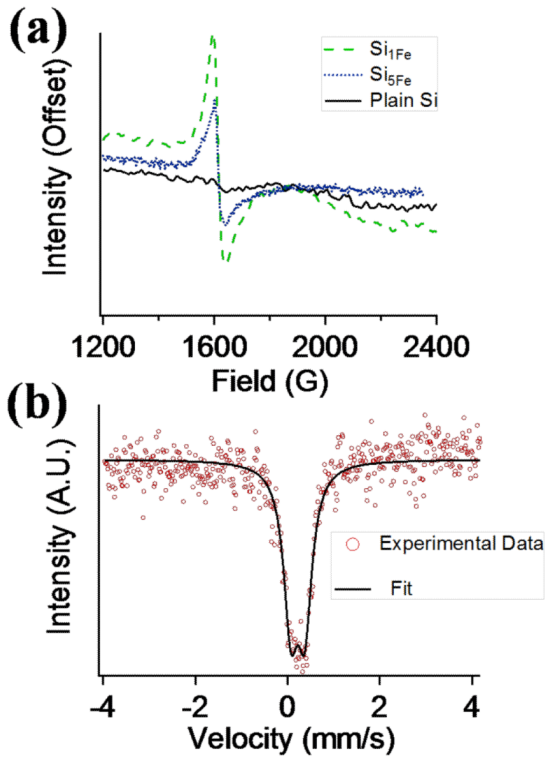

Figure 4.

(a) X-band EPR spectra for Si_{1Fe} (dashed line) and Si_{5Fe} (dotted line). For comparison, the EPR spectrum for undoped silicon nanoparticles is also included (solid line); **(b)** Mössbauer spectrum of Si_{5Fe} nanoparticles fits to the parameters specific to the Fe^{3+}.

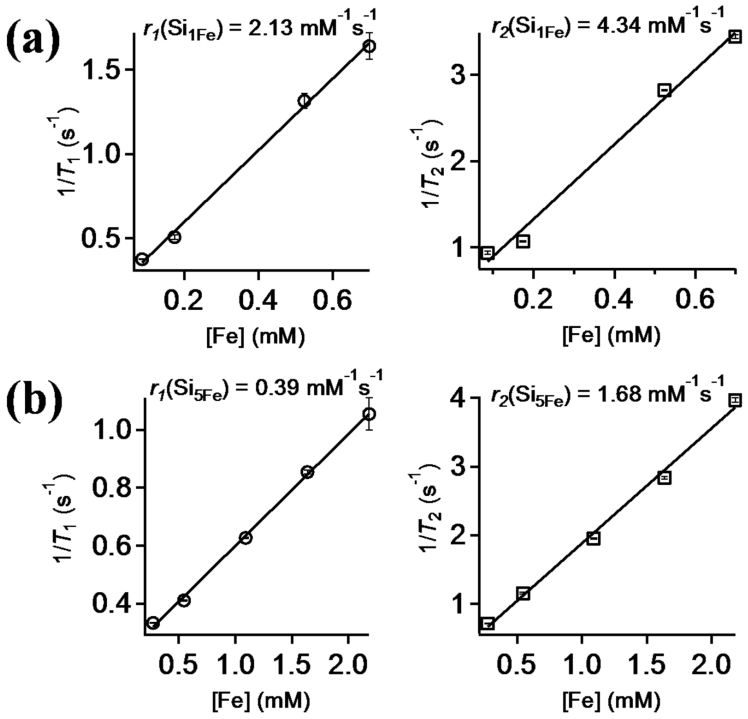

Figure 5.
Relaxivity plots for **(a)** Si_{1Fe} and **(b)** Si_{5Fe} dissolved in water and measured at 37 °C (n=3).

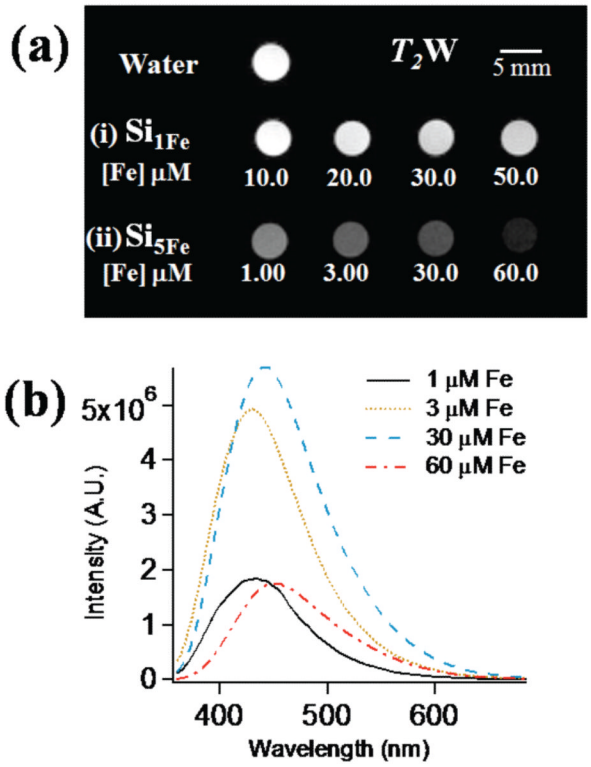

Figure 6.

(a) T_2-weighted MRI images for (i) Si_{1Fe} and (ii) Si_{5Fe} nanoparticles dissolved in water; **(b)** Emission intensity of the same Si_{5Fe} samples from (a) measured at λ_{ex} = 350 nm.

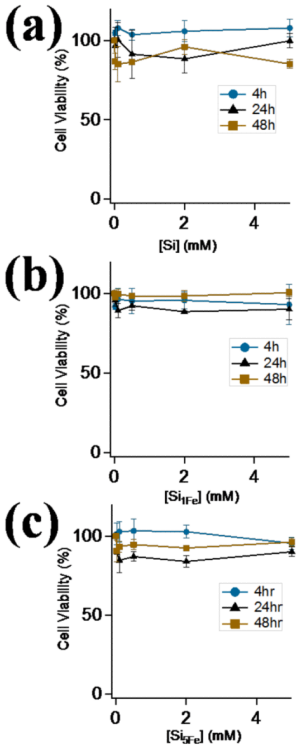

Figure 7.

Cell viability for HepG2 cells when incubated with amine terminated **(a)** undoped Si, **(b)** Si_{1Fe} and **(c)** Si_{5Fe} nanoparticles at concentrations ranging from 0-5.0 mM for 4 h, 24 h and 48 h (n=3). At the highest concentrations with longest incubation hours the cells exhibit ≥ 85% viability.

Table 1

Particle size (diameter), quantum yield (Q.Y.) and the iron content (mole %) for Si_{xFe} nanoparticles dispersed in nanopure water

Sample	Particle Size (nm)	Q.Y. (%)	Fe content (mole %)
Si_{1Fe}	2.91±0.99	15.0±1.00	0.60±0.20
Si_{5Fe}	2.87±1.21	10.0±1.50	0.90±0.10
Si_{10Fe}	3.01±1.10	1.00±0.05	0.50±0.15